

Dielectric, modulus and impedance analysis of lead-free ceramics $\text{Ba}_{0.8}\text{La}_{0.133}\text{Ti}_{1-x}\text{Sn}_x\text{O}_3$ ($x = 0.15$ and 0.2)

F.I.H. Rhouma · A. Dhahri · J. Dhahri · M.A. Valente

Received: 2 February 2012 / Accepted: 10 April 2012 / Published online: 1 May 2012
© The Author(s) 2012. This article is published with open access at Springerlink.com

Abstract Titanate barium (BaTiO_3)-type oxide ceramics $\text{Ba}_{0.8}\text{La}_{0.133}\text{Ti}_{1-x}\text{Sn}_x\text{O}_3$ (BLTS) (here $x = 0.15$ and 0.2) have been synthesized by the standard solid-state reaction method. Preliminary room temperature X-ray study confirms the formation of single-phase compounds in a rhombohedral crystal system. The electrical properties of BLTS were studied using the ac impedance spectroscopy technique over a wide range of temperature (120–320 K) in the frequency range of 40 Hz to 10 MHz. The presence of a single arc in the complex modulus spectrum at different temperatures confirms the single-phase character of the BLTS compounds.

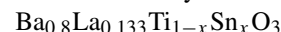
1 Introduction

The most important ferroelectric ceramics crystallize in the ABO_3 structured perovskite. The flexible structure of perovskite shows diverse physical properties which are interesting for functional applications [1–4]. It has already been established that a wide range of complex compounds, obtained by single- or multi-element doping at the A and/or B sites of the perovskite structure, are potentially suitable for applications such as transducers, sensors, electro-optic modulators, memory components and many other active

and passive devices [5–8]. The researchers paid more attention to improve the dielectric properties of pure BaTiO_3 via partial substitution of either Ba-ions (A-site doping) or Ti-ions (B-site doping), which may result in high permittivity, high piezoelectric and ferroelectric properties; the absence of lead increases their application as non-polluting materials [9]. So far, many new materials with excellent properties have been developed, such as $\text{Ba}_{1-x}\text{Sr}_x\text{TiO}_3$ [10], $\text{BaTi}_{1-x}\text{Sn}_x\text{O}_3$ [11–13] and $(\text{BaSr})(\text{SnTi})\text{O}_3$ [14, 15] ceramics. Research is now on the way in producing such lead-free ceramics with relaxing behavior at room temperature which are of great interest for a wide range of applications [16–22]. In view that the important properties exhibited by the materials and also their conductivity and impedance spectroscopy studies have not yet been reported in the literature, an attempt has been made to study the structural, electrical properties of $\text{Ba}_{0.8}\text{La}_{0.133}\text{Ti}_{1-x}\text{Sn}_x\text{O}_3$ ceramics. The permittivity (ϵ^*), impedance (Z^*), electrical modulus (M^*), and conductivity (σ^*) spectroscopy techniques have been studied over the wide range of temperature (120–320 K) and frequency (40 Hz to 10 MHz).

2 Experimental details

2.1 Ceramic route synthesis of phases

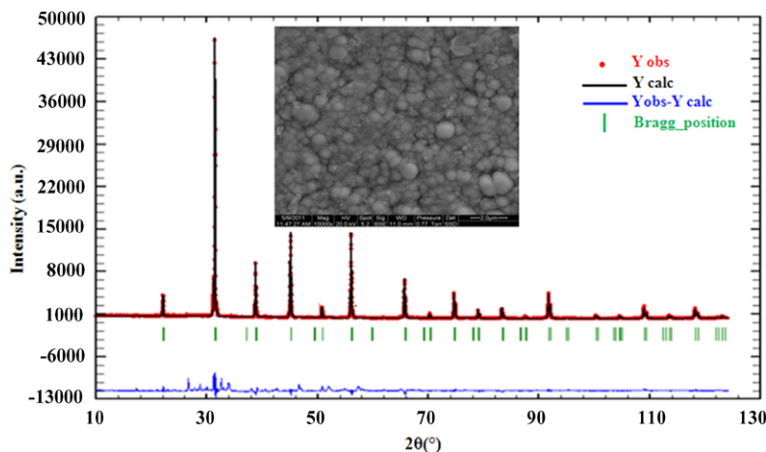


The polycrystalline compounds of $\text{Ba}_{0.8}\text{La}_{0.133}\text{Ti}_{1-x}\text{Sn}_x\text{O}_3$ (where $x = 0.15$ and 0.2) were prepared by the standard solid-state reaction method using high purity (more than 99.9 %) starting compounds such as BaCO_3 , La_2O_3 , TiO_2 and SnO_2 . All the samples were preheated before weighing. The initial mixtures of ingredients were thoroughly grounded and calcined at 1173 K for 24 hours in a muffle

F.I.H. Rhouma (✉) · A. Dhahri · J. Dhahri
Faculté des Sciences de Monastir, Département de Physique,
Unité de Recherche de Physique des Solides, 5019 Monastir,
Tunisia
e-mail: rhouma.feten@yahoo.fr
Fax: +216-73-500278

M.A. Valente
I3N and Physics Department, University of Aveiro,
3810-193 Aveiro, Portugal

Fig. 1 Observed (*solid circles*) and calculated (*solid line*) XRD patterns of $\text{Ba}_{0.8}\text{La}_{0.133}\text{Ti}_{0.85}\text{Sn}_{0.15}\text{O}_3$ samples obtained at room temperature. The difference between these spectra is plotted at the room temperature. Bragg reflections are indicated by ticks. The *inset* represents the SEM micrograph of the sample



furnace. The resultant powders were taken out, re-ground thoroughly and pressed into pellets. The pellets were sintered at 1673 K for 3 hours each with intermediate re-grinding and pelletization.

2.2 Material characterization

The determination of lattice parameters of the unit cell structure and identification of phase were carried out at room temperature by powder X-ray diffraction (XRD) technique recorded by Siemens D-5000 diffractometer (Cu K_α radiation). These XRD patterns were calculated by the Rietveld method to obtain the structure model with the least deviation. Surface morphology of the sintered samples was examined by scanning electron microscope (SEM, Philips XL30 with an energy dispersive X-ray spectrometer). Afterwards, a pellet of about 4 mm in diameter and 1 mm in thickness was used for the electrical measurements. Dielectric response from 120 up to 320 K was measured using Agilent 4294 A impedance analyzer at frequencies from 40 Hz to 10 MHz.

3 Results and discussion

3.1 SEM observations

The morphology and the grain size of samples were examined by SEM. The inset of Fig. 1 shows a typical SEM image of the composition specimen of $x = 0.15$. The image shows homogenous grains distributed over the entire volume of the sample and a good crystallization. The average grain size decreases from 298.79 nm for $x = 0.15$ to 291.2 nm for $x = 0.2$, depending on the Sn^{4+} content.

3.2 Structural properties

The powder X-ray diffraction patterns of the polycrystalline ceramic samples $\text{Ba}_{0.8}\text{La}_{0.133}\text{Ti}_{1-x}\text{Sn}_x\text{O}_3$ collected

at room temperature are shown in Fig. 1. The figure presents the measured, calculated (refined) X-ray diffraction pattern and positions of Bragg reflections for the sample $\text{Ba}_{0.8}\text{La}_{0.133}\text{Ti}_{0.85}\text{Sn}_{0.15}\text{O}_3$ as an example of this series. As can be seen from the figure, all the reflection peaks of the X-ray profile are indexed and lattice parameters are determined using a least-squares method with the help of a standard program (Wintplor [23]). On the basis of the best agreement between calculated (cal) and observed (obs) results, a suitable unit cell of the compound in the rhombohedra system with space group $R\bar{3}c$ was selected. Using the refined crystallographic data, the unit cell parameters and other fitting parameters of all the samples were computed and are reported in Table 1. For two samples, the distortion ratio (c/a) is high as compared with the parent BaTiO_3 (2.444). Such a significant increase exists due to the substitution of either Ba-ions by La or Ti-ions by Sn in perovskite BaTiO_3 , since these substituted ions have large variation in ionic radii, i.e., (La^{3+} (1.22 Å) and Sn^{4+} (0.69 Å)), with parent BaTiO_3 (Ba^{2+} (1.216 Å) and Ti^{4+} (0.605 Å)) [24].

3.3 Impedance spectroscopy

The complex impedance spectroscopy (CIS) technique [25] was used to analyze the electrical response (i.e., transport properties) of a polycrystalline sample in a wide range of frequency at different temperatures. The CIS gives the direct correlation between the response of a real system and an idealized model circuit composed of discrete electrical components. Figure 2 shows temperature-dependent spectra (Nyquist plot) of BLTS samples. The impedance spectrum is distinguished by semicircles. A single semicircle indicates that only one primary mechanism exists for the electrical conduction within the samples at $120 \text{ K} < T < 320 \text{ K}$. The depressed semicircles have their centers on a line below the real axis, which indicates departure from the ideal Debye behavior [25]. The absence of second semicircle in the complex impedance plots suggests the dominance of bulk con-

Table 1 Applied conditions and results of refinement by Rietveld method

Experimental conditions for crystallographic data collection		
Radiation	Cu K α ($\lambda = 1.5406 \text{ \AA}$)	
Measuring range ($^\circ$)	$10 < 2\theta < 130$	
Step	(2θ) : 0.016°	
Integration time	17 s	
Programme d'affinement	Fullprof	
Rietveld data		
BLTSx	BLTS0.15	BLTS0.2
Symmetry	Rhombohedral	Rhombohedral
Space group	R $\bar{3}c$	R $\bar{3}c$
Lattice parameter and volume	$a = b = 5.69 \text{ \AA}, c = 13.92 \text{ \AA}, V = 390.67 \text{ \AA}^3$	$a = b = 5.70 \text{ \AA}, c = 13.94 \text{ \AA}, V = 405.9 \text{ \AA}^3$
Ratio (c/a)	2.446	2.445
R_{Bragg} (%)	4.3	3.1
R_F (%)	5.5	4.5
χ^2 (%)	3.2	2.4

tributions in the BLTS compounds [26]. With increasing the temperature, intercept point on the real axis shifts toward the origin indicating the decrease in the resistive property of the material. The experimental impedance spectra were simulated by the impedance of equivalent circuit composed of bulk resistance R_p and constant phase CPE elements connected in parallel (see Fig. 3). The CPE, defined by two values, CPE-T and CPE-P, is expressed by the following equation:

$$Z = \frac{1}{[T(j\omega)^P]} \quad (1)$$

where T (CPE-T) is expressed in units of capacitance component and ω is angular frequency ($\omega = 2\pi f$). The CPE is identical to a capacitance component when the exponent P (CPE-P) equals 1, to a resistance component when $P = 0$, and to a Warburg element when $p = 0.5$. When the CPE is placed in parallel to a resistance, a Cole element (depressed semicircle) is produced. The expressions of real (Z') and imaginary (Z'') components of impedance related to the equivalent circuit are:

$$Z' = \frac{R_p(1 + R_p T \omega^P \cos(\frac{p\pi}{2}))}{(1 + R_p T \omega^P \cos(\frac{p\pi}{2}))^2 + (R_p T \omega^P \sin(\frac{p\pi}{2}))^2} \quad (2)$$

$$-Z'' = \frac{R_p^2 T \omega^P \sin(\frac{p\pi}{2})}{(1 + R_p T \omega^P \cos(\frac{p\pi}{2}))^2 + (R_p T \omega^P \sin(\frac{p\pi}{2}))^2} \quad (3)$$

The parameters of each fitting are summarized in Table 2 and were determined using a non-linear least-squares fitting. Here, it is noted that the values of R_p , resistances of each of the BLTS composition, exhibit decreasing trend with the increase in temperature. It indicates that the conductivity increases with increase in temperature supporting the typical

negative temperature coefficient of resistance behavior (i.e., NTCR) of the materials usually shown by semiconductors. As the values of p vary in the range 0.9–1 confirming the weakness interaction between localized sites, the conductivity σ_p is obtained from R_p by means of the relation

$$\sigma_p = \frac{e}{S R_p} \quad (4)$$

Here e is the thickness and S the effective area of the investigated material. The electrical conductivity dependence on temperature is shown in Fig. 4 in the form of $\ln(\sigma_{\text{dc}})$ versus $(1/T)$ plot. Following the Arrhenius law, the obtained activation energies are $E_p = 0.1$ eV in region I ($T > 238$ K) and 0.018 eV in region II ($T < 238$ K) for $x = 0.15$, and $E_p = 0.1$ eV in region I ($T > 232$ K) and 0.017 eV in region II ($T < 232$ K) for $x = 0.2$.

3.4 Electrical conductivity analysis

The study of frequency-dependent conductivity is a well-established method for characterizing the hopping dynamics of the charge carrier/ions. Variation of conductivity σ of the sample Ba_{0.8}La_{0.133}Ti_{0.85}Sn_{0.15}O₃ as a function of frequency at several temperatures (120–320 K) is depicted in Fig. 5. The conductivity plots show significant frequency dispersion at lower frequencies that shifts to higher frequency with increase in temperature, quite similar to the vast majority of solids. Extrapolating these conductivity curves at lower frequencies gives the DC conductivity. At the high-frequency end, the curves approach each other, once again indicating the possibility of the presence of space charges [27]. A basic fact about the conductivity is that σ increases

with frequency (any hopping model has this feature). The observed frequency-independent σ_{dc} is explained by the relaxation jump model [28]. According to this model, at low

frequencies and/or higher temperatures, conduction occurs through hopping of charged particles from one localized state to another resulting in long-range translational motion of charge carriers contributing to σ_{dc} . Conductivities in a variety of perovskite oxides have long been found to obey a power law proposed by Jonscher [28]:

$$\sigma = \sigma_{dc} + \sigma_{ac}(\omega) = \sigma_{dc} + A\omega^s \tag{5}$$

where $\sigma(\omega)$, σ_{dc} and $\sigma_{ac}(\omega)$ have the usual meaning, A is a constant and s is the power exponent that can take values less than 1 [29]. The transport mechanism is explained by the thermally activated hopping process between two sites separated by an energy barrier. Equation (5) was used to fit the conductivity data. In the fitting procedure, the A and s values have been varied simultaneously to get the best fits.

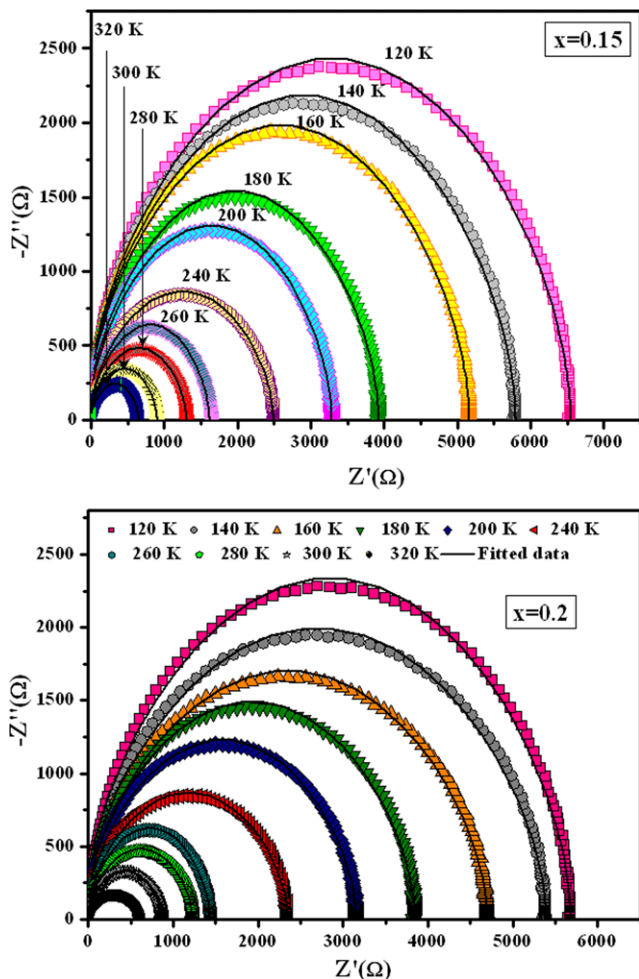


Fig. 2 Experimental and simulated semicircles plot at different temperatures for the samples $Ba_{0.8}La_{0.133}Ti_{0.85}Sn_{0.15}O_3$ and $Ba_{0.8}La_{0.133}Ti_{0.80}Sn_{0.2}O_3$

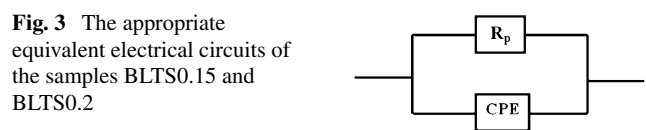


Fig. 3 The appropriate equivalent electrical circuits of the samples BLTS0.15 and BLTS0.2

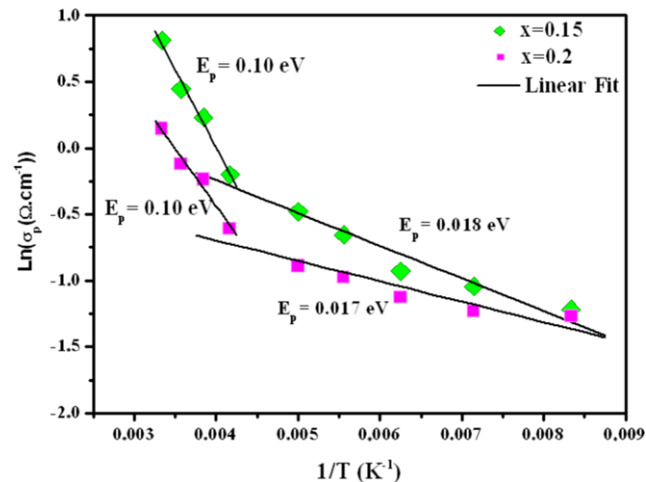


Fig. 4 Arrhenius plot of σ_p versus $1/T$ for the samples $Ba_{0.8}La_{0.133}Ti_{0.85}Sn_{0.15}O_3$ and $Ba_{0.8}La_{0.133}Ti_{0.80}Sn_{0.2}O_3$

Table 2 The estimated values of the equivalent circuits' parameters

T (K)	$x = 0.15$		$x = 0.2$	
	R_p (Ω)	CPE-T (nF)	R_p (Ω)	CPE-T (nF)
120	6404.40	8.53	5548.50	2.71
140	5662.21	11.5	5264.69	2.83
160	5044.24	12.99	4590.47	3.27
180	3835.62	17.08	3760.02	3.80
200	3211.19	20.39	3081.79	4.88
240	2433.54	26.92	2303.51	6.53
260	1580.23	41.45	1405.14	10.17
280	1275.33	50.25	1200.52	12.53
300	882.69	71.42	840.36	17.90
320	637.05	98.90	588.25	25.57

However, similar observations have been made by Cramer [30] and Papathanassiou [31, 32]. Figure 6 shows the variation of σ as a function of frequency at the temperature $T = 120$ K for Ba_{0.8}La_{0.133}Ti_{1-x}Sn_xO₃ ($x = 0.15$ and 0.2) compounds. These curves reveal an increase of the conductivity when increasing the Sn doping concentration. In Table 3 we have presented the values of σ_{dc} , A and s of BLTS0.15 and BLTS0.2 determined at the temperature $T = 120$ K. From

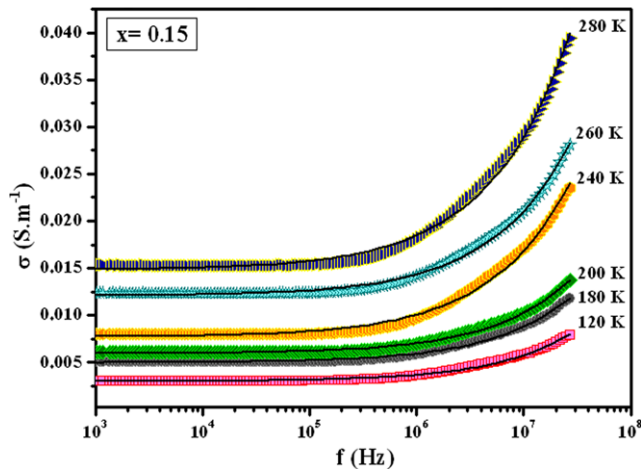


Fig. 5 Frequency dependence of the conductivity (σ) of Ba_{0.8}La_{0.133}Ti_{0.85}Sn_{0.15}O₃ at different temperatures. *Solid lines* are the fitting to the experimental data using universal Jonscher's power law

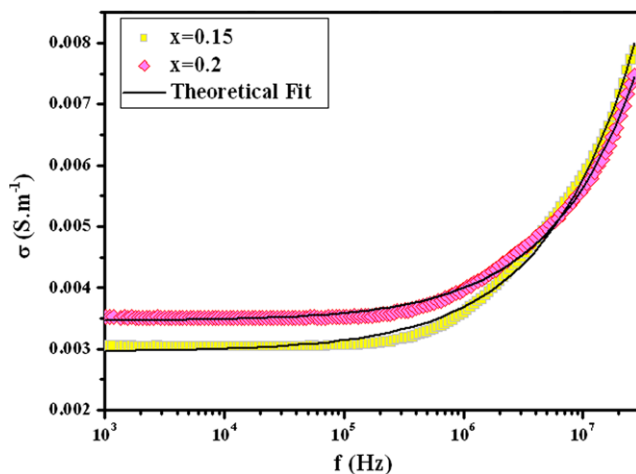


Fig. 6 Frequency dependency of conductivity of BLTS0.15 and BLTS0.2 at $T = 120$ K

Table 3 Values of the dc conductivity (σ_{dc}), the constant (A), the slope (s) and the activation energies E_{dc} for Ba_{0.8}La_{0.133}Ti_{1-x}Sn_xO₃ ($x = 0.15$ and 0.2) compounds determined at the temperature $T = 120$ K

Composition	σ_{dc}	A (10^{-7})	s	E_{dc} (I) (eV)	E_{dc} (II) (eV)
BLTS0.15	0.0029	2.263	0.605	0.1	0.099
BLTS0.2	0.0034	1.254	0.585	0.02	0.014

the table we can conclude that σ_{dc} and s increase while A decreases when increasing the Sn doping concentration. DC conductivity data are plotted in Arrhenius format as $\ln(\sigma_{dc})$ vs. $1/T$ for all the samples (see Fig. 7), and show Arrhenius-type behavior described by $\sigma_{dc} = \sigma_0 \exp(-\frac{E_{dc}}{k_B T})$, where σ_0 is the pre-exponential factor corresponding to $1/T = 0$, E_{dc} is the activation energy for charge transfer, k_B the Boltzmann constant and T the absolute temperature [33]. The activation energy values, for samples with different Sn concentrations calculated from the plot of $\ln(\sigma_{dc})$ vs. $1/T$ are listed in Table 3. These values match nicely with the values from Eq. (4). The obtained values suggest that the conduction is created by thermally activated mechanism.

3.5 Complex permittivity representation

The study of the dielectric properties is another important source of valuable information about conduction processes since it can be used to understand the origin of the dielectric losses, the electrical and dipolar relaxation time [34]. It is observed that the complex permittivity data of our samples obey the Cole–Cole equation [35]:

$$\varepsilon^* = \varepsilon' + i\varepsilon'' = \varepsilon_\infty + \frac{\varepsilon_s - \varepsilon_\infty}{1 + (i\omega\tau)^{1-\alpha}} - i \frac{\sigma_{dc}}{\varepsilon_0\omega} \quad (6)$$

Here, ε_s and ε_∞ are the dielectric constants on low and high frequency sides of the relaxation, ω is the angular frequency τ is the mean relaxation time instead of the single

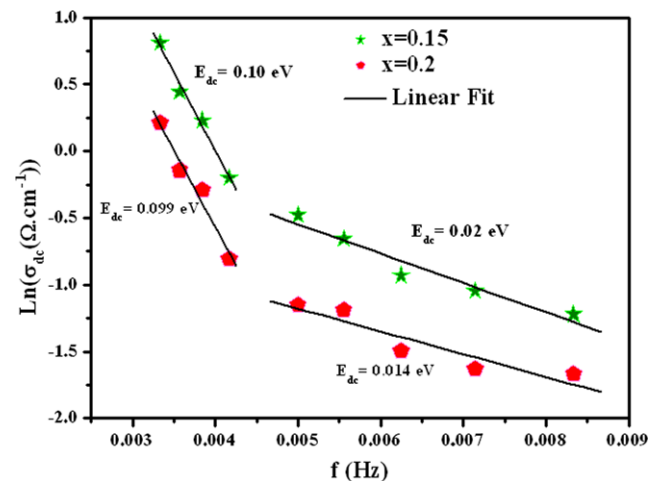
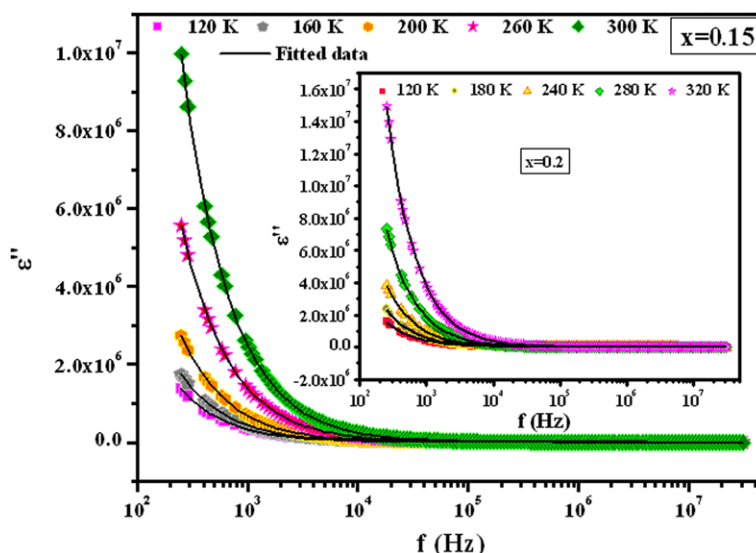


Fig. 7 Plot of dc conductivity vs. $1/T$. The *open symbols* are experimental data points and the *solid lines* are the least-squares straight-line fit

Fig. 8 Variation of the imaginary part of dielectric constant vs. frequency for of (Ba_{0.8}La_{0.133}Ti_{1-x}Sn_xO₃) ceramic where $x = 0.15$ and 0.2 at various temperatures



relaxation time of pure Debye process while the Cole–Cole parameter α indicates the width of the relaxation time distribution and provides a measure of the polydispersive nature. The last term at the right-hand-side is due to the high conducting behavior contributing only to the imaginary part [36], which is due to the displacement of charge carriers, rather than the effect of polarization mechanism.

Consequently, the complex permittivity may be decomposed into real and imaginary parts, i.e.

$$\begin{aligned} \epsilon'(\omega) = & \frac{(\epsilon_s - \epsilon_\infty)(\omega\tau_1)^{1-\alpha} \cos((1-\alpha)\frac{\pi}{2})}{1 + 2(\omega\tau_1)^{1-\alpha} \cos((1-\alpha)\frac{\pi}{2}) + (\omega\tau_1)^{2(1-\alpha)}} \\ & + \frac{\sigma_{dc}}{\omega\epsilon_0} \end{aligned} \tag{7}$$

and

$$\begin{aligned} \epsilon''(\omega) = & \frac{(\epsilon_s - \epsilon_\infty)(\omega\tau_1)^{1-\alpha} \sin((1-\alpha)\frac{\pi}{2})}{1 + 2(\omega\tau_1)^{1-\alpha} \cos((1-\alpha)\frac{\pi}{2}) + (\omega\tau_1)^{2(1-\alpha)}} \\ & + \frac{\sigma_{dc}}{\omega\epsilon_0} \end{aligned} \tag{8}$$

Figure 8 shows the frequency dependence of the imaginary part (ϵ'') of dielectric constant at different temperatures for the samples BLTS0.15 and BLTS0.2. Analysis of experimental data was carried out on the basis of Eq. (8). No loss peak are observed in the ϵ'' spectra. The high values of ϵ'' and especially at high temperatures and the large drop of ϵ'' when the frequency increases seem to indicate the influence of conductivity and space charge polarization mask the ferroelectric relaxation. Thus, the observed dielectric dispersion at low frequency may be due to the polarization mechanism associated with the thermally activated conduction of mobile ions and/or other defects. Similar behavior has been reported by Kamal et al. [37] on the sample of Ba(Al_{1/2}Nb_{1/2})O₃.

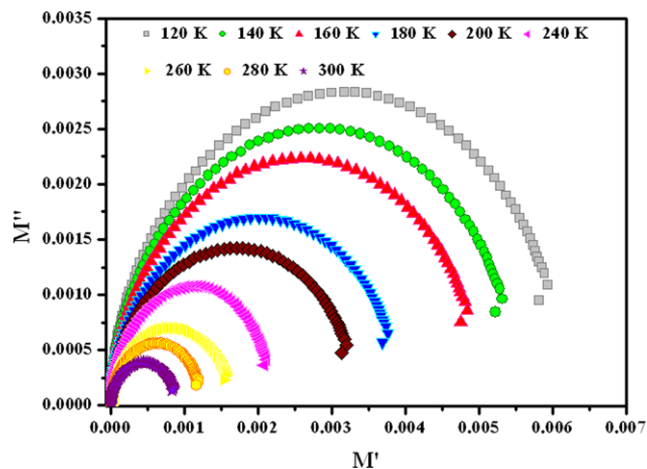
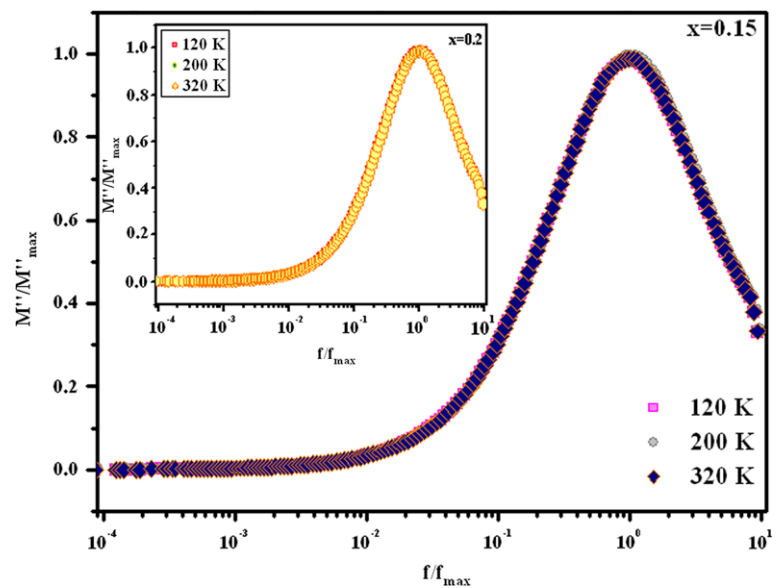


Fig. 9 Variation of M'' versus M' of Ba_{0.8}La_{0.133}Ti_{0.85}Sn_{0.15}O₃ at selected temperatures

3.6 Electric modulus studies

The impedance data can be analyzed in a much better way by replottting the data in the complex modulus (M^*) formalism, which is based on the polarization analysis. The electric modulus (M^*) is defined as $M^* = M' + jM'' = 1/\epsilon^* = j\omega C_0 Z^*$, where M' (real part) = $\omega C_0 Z''$ and M'' (imaginary part) = $\omega C_0 Z'$ (ω = angular frequency i.e., $2\pi f$), (C_0 = geometrical capacitance = $\epsilon_0 S/e$), (ϵ_0 = permittivity of free space). The temperature dependence of the complex modulus spectrum (M'' vs. M') of BLTS0.15 compounds is shown in Fig. 9. From this figure, we can notice that the samples modulus spectrum has a typical semi-circle pattern with its center lying below the real axis (unlike the ideal Debye type response). This is evident from the shape of the deformed arcs with their centers positioned

Fig. 10 Modulus master curve of $\text{Ba}_{0.8}\text{La}_{0.133}\text{Ti}_{0.85}\text{Sn}_{0.15}\text{O}_3$ material



below the x -axis [38]. The presence of a single semicircular arc confirms the single phase formation of the compounds.

Scaling behavior of the samples was studied by replotting normalized parameters (i.e. M''/M''_{\max}) versus (f/f_{\max}) ; f_{\max} is frequency corresponding to M''_{\max} at different temperatures (Fig. 10). The modulus scaling behavior gives an insight into the dielectric processes occurring inside the material. The low frequency side of the peak in M''/M''_{\max} versus f/f_{\max} curve represents the range of frequencies in which the charge carriers can move over a long distance (i.e. charge carriers can perform successful hopping from one site to the neighboring site). The high frequency side of M''/M''_{\max} versus f/f_{\max} curve represents the range of frequencies in which the charge carriers are spatially confined to their potential wells, and thus could make localized motions inside the well. The region where the peak occurs is an indication of the transition from long-range to short-range. The perfect overlapping of all the curves at different temperatures suggests that all possible relaxation mechanisms occurring at different frequencies exhibit the same thermal energy and the dynamical processes are temperature-independent [39]. The modulus plot can be characterized by full width at half height or in terms of a non exponential decay function [40, 41] $\varphi(t) = \exp\{-(\frac{t}{\tau})^\beta\}$, where τ is a characteristic time and β is a non-exponential parameter representative of a distribution of relaxation time. The value of β is positioned in the range $0 < \beta < 1$, which represents the departure from the linear exponential ($\beta = 1$). The β value can be determined by knowing the full width-at-half-maximum (FWHM) of the M''/M''_{\max} spectrum ($\beta = 1.14/\text{FWHM}$). In our case, the values of β estimated for BLTS0.15 and BLTS0.2 are 0.2 and 0.19 respectively. This indicates that the relaxation process for all the tested samples is of non-Debye-type relaxation phenomena in good

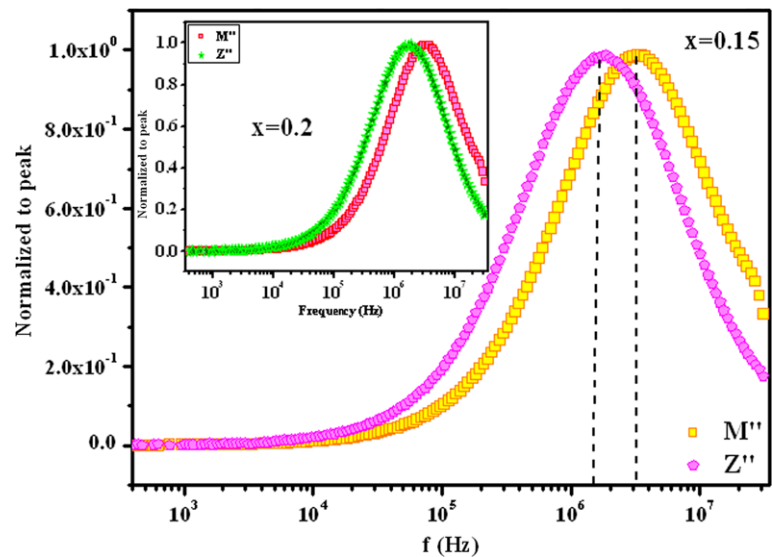
agreement with the observations from complex permittivity spectrum.

A comparison of the impedance with the electric modulus data allows the determination of the bulk response in terms of localized or non-localized conduction [42]. In Fig. 11, the normalized parameters M''/M''_{\max} and Z''/Z''_{\max} for the composition $x = 0.15$ and 0.2 as a function of frequency at 120 K are shown. The overlapping of peak positions of the M''/M''_{\max} and Z''/Z''_{\max} curves is an evidence of delocalized or long-range relaxation [42]. However, for the present system the M''/M''_{\max} and Z''/Z''_{\max} peaks do not overlap but are very close, suggesting the components from both long-range localized relaxations.

4 Conclusion

A new composition of BLTS ($\text{Ba}_{0.8}\text{La}_{0.133}\text{Ti}_{1-x}\text{Sn}_x\text{O}_3$) was prepared in a single phase by a solid-state reaction technique. The investigations of ($\text{Ba}_{0.8}\text{La}_{0.133}\text{Ti}_{1-x}\text{Sn}_x\text{O}_3$) by Rietveld analysis indicate that these samples crystallize in rhombohedral structure with $R\bar{3}c$ like a space group. Impedance spectroscopy is used to study the dielectric relaxation (conduction) for the synthesized samples. Interpretation of impedance data in the light of their ideal equivalent circuits confirmed that the vacancy diffusion in the microstructure for $\text{Ba}_{0.8}\text{La}_{0.133}\text{Ti}_{1-x}\text{Sn}_x\text{O}_3$ ($x = 0.15$ and 0.2) ceramics is a thermally activated process. The frequency-dependent conductivity plots show two regions of conduction process, i.e., a low frequency region due to DC conduction and a high-frequency region due to localized hopping and/or reorientational motion. Modulus analysis confirmed the single-phase behavior of materials in a good agreement

Fig. 11 Frequency (angular) dependence of normalized peaks, M''/M''_{\max} and Z''/Z''_{\max} , for BLTS0.15 and BLTS0.2 at 120 K



with the information received from XRD study. The activation energies calculated both from impedance and electric modulus spectra are comparable.

Open Access This article is distributed under the terms of the Creative Commons Attribution License which permits any use, distribution, and reproduction in any medium, provided the original author(s) and the source are credited.

References

- C.H. Ahn, J.M. Triscone, J. Mannhart, *Nature (London)* **424**, 1015 (2003)
- O. Auciello, J.F. Scott, R. Ramesh, *Phys. Today* **51**, 22 (1998)
- K. Dorr, *J. Phys. D* **39**, R125 (2006)
- B.N. Mbenkum, N. Ashkenov, M. Schubert, M. Lorenz, H. Hochmuth, D. Michel, M. Grundmann, G. Wagner, *Appl. Phys. Lett.* **86**, 091904 (2005)
- L.H. Parker, A.F. Tasch, *IEEE Circuits Devices Mag.* **6**, 17 (1990)
- T. Kawaguchi, H. Adachi, K. Setsune, O.Y. Amazaki, K. Wasa, *Appl. Opt.* **23**, 2187 (1984)
- K.K. Deb, *Ferroelectrics* **82**, 45 (1998)
- L.A. Thomas, *Ferroelectrics* **3**, 231 (1972)
- J. Qi, Z. Gui, W. Li, Y. Wang, Y. Wu, L. Li, *Mater. Lett.* **56**, 507 (2002)
- J.W. Liou, B.S. Chiou, *Mater. Chem. Phys.* **51**, 59 (1997)
- X. Wei, Y. Feng, L. Hang, X. Yao, *Ceram. Int.* **30**, 1401 (2004)
- X. Wang, B. Li, *J. Solid State Commun.* **149**, 537 (2009)
- V.V. Shvartsman, W. Kleemann, J. Dec, *J. Appl. Phys.* **99**, 124111 (2006)
- S. Lu, Z. Xu, *Appl. Phys. Lett.* **92**, 232907 (2008)
- I.A. Souza, L.S. Cavalcante, J.C. Sczancoski, F. Moura, C.O. Paiva-Santos, J.A. Varela, A.Z. Simoes, E. Longo, *J. Alloys Compd.* **477**, 877 (2009)
- L.E. Cross, *Ferroelectrics* **76**, 241 (1987)
- J. Ravez, C. Broustera, A. Simon, *J. Mater. Chem.* **9**, 1609 (1999)
- F. Bahri, A. Simon, H. Khemakhem, J. Ravez, *Phys. Status Solidi* **184**, 2 (2001) 459
- A. Simon, J. Ravez, *Solid State Sci.* **5**, 1459 (2003)
- A. Aydi, H. Khemakhem, C. Boudaya, R. Von Der Muhll, A. Simon, *Solid State Sci.* **6**, 333 (2004)
- H. Abdelkefi, H. Khemakhem, G. Velu, J.C. Carru, R. Von Der Muhll, *J. Alloys Compd.* **399**, 1 (2005)
- N. Abdelmoula, H. Chabaane, H. Khemakhem, R. Von Der Muhll, A. Siumon, *Phys. Stat. (a)* **203**, 987 (2006)
- H.M. Rietveld, *J. Appl. Crystallogr.* **2**, 65 (1969)
- R.D. Shannon, *Acta Crystallogr. A* **32**, 75 (1976)
- J. Rossac Donald, *Impedance Spectroscopy* (Wiley, New York, 1987)
- S. Sen, R.N.P. Choudhary, *Mater. Chem. Phys.* **87**, 256 (2004)
- A.R. James, K. Srinivas, Low temperature and impedance spectroscopy of PMN-PT ceramics. *Mater. Res. Bull.* **34**, 1301 (1999)
- A.K. Jonscher, *Universal Relaxation Law* (Chelsea Dielectrics Press, London, 1996)
- R.H. Chen, R.Y. Chang, S.C. Shern, *J. Phys. Chem. Solids* **63**, 2069 (2002)
- Z.C. Cramer, S. Brunklaus, E. Ratai, Y. Gao, *Phys. Rev. Lett.* **91**, 266601 (2003)
- A.N. Papanthassiou, *J. Mater. Lett.* **59**, 1634 (2005)
- A.N. Papanthassiou, *J. Phys. Chem. Solids* **66**, 1849 (2005)
- S. Kumar, K.B.R. Varma, *Solid State Commun.* **146**, 137 (2008)
- R. Ayouchi, D. Leinen, F. Martin, M. Gabas, E. Dalchiele, J.R. Ramos-Barrado, *Thin Solid Films* **426**, 68 (2003)
- D.K. Pradhan, R.N.P. Choudhary, B.K. Samantary, *Int. J. Electrochem. Sci.* **3**, 597 (2008)
- K.C. Kao, *Dielectric Phenomena in Solids* (Elsevier/Academic Press, Amsterdam/San Diego, 2004)
- K. Prasad, K.P. Chandra, S. Bhagat, S.N. Choudhary, A.R. Kulkarni, *J. Am. Ceram. Soc.* **93**, 190 (2010)
- A. Shukla, R.N.P. Choudhary, A.K. Thakur, D.K. Pradhan, *Physica B* **405**, 99 (2010)
- S. Saha, T.P. Sinha, *Phys. Rev. B* **65**, 134103 (2002)
- R. Kohlrausch, *Prog. Annu.* **123**, 393 (1847)
- G. Williams, D.C. Watts, *Trans. Faraday Soc.* **66**, 80 (1970)
- R. Gerhardt, *J. Phys. Chem. Solids* **55**, 1491 (1994)